

Novel selenium and/or copper substituted hydroxyapatite–gelatin–chitosan–eggshell membrane nanocomposite scaffolds for bone tissue engineering applications

Journal of Applied Biomaterials &
Functional Materials
1–8


© The Author(s) 2023

Article reuse guidelines:

sagepub.com/journals-permissions

DOI: 10.1177/22808000231187959

journals.sagepub.com/home/jbf

Sara Ibrahim Korowash^{1,2}, Nik SA Nik Sharifulden²,
Doreya Mohamed Ibrahim¹ and David YS Chau² 

Abstract

Limitations with the majority of bone therapeutic treatments include low availability, ethical constraints and low biological compatibility. Although a number of choice materials have been exploited successfully, there has always been scope for improvement as well as development of the next-generation of materials. Herein, scaffolds – developed from gelatin, chitosan and eggshell membranes – were crosslinked using tannic acid, and further infused with selenium and/or copper substituted hydroxyapatite nanoparticles to generate a novel nanocomposite substrate. FESEM images of the nanocomposite scaffolds revealed the presence of interconnected pores, mostly spread over the whole surface of the scaffold, alongside XRD and FTIR profiling that detailed the formation of hydroxyapatite as a sole phase. Moreover, physical characterisation of the nanocomposite confirmed that the hydroxyapatite particulates and the eggshell membrane fibres were uniformly distributed and contributed to the surface roughness of the scaffold. Biocompatibility and cytotoxicity of the novel constructs were assessed using the mouse-derived osteoblastic cell line, MC3T3-E1, and standard cell culture assays. Metabolic activity assessment (i.e. MTS assay), LDH-release profiles and Live/Dead staining demonstrated good cell adhesion, viability, and proliferation rates. Accordingly, this work summarises the successful development of a novel construct which may be exploited as a clinical/therapeutic treatment for bone repair as well as a possible translational application as a novel biomaterial for the drug development pipeline.

Keywords

Selenium and/or copper substituted hydroxyapatite, gelatin, chitosan, eggshell membrane, tannic acid, scaffold

Date received: 29 March 2023; revised: 10 June 2023; accepted: 20 June 2023

Introduction

Synthetic bone substitute, the main calcium phosphate compound that naturally occurs in bone and dental mineralised tissues, is utilised in bone repair. It is the most frequently synthesised product, hydroxyapatite: (HA; $\text{Ca}_{10}(\text{PO}_4)_6(\text{OH})_2$), fabricated in different forms including; granules, cements, pastes and geometric blocks, employed in biomaterial engineering.^{1,2} Therefore, in order to fill osseous tissue deficiencies, administer medications are directly applied to the bone tissue. The structure of

hydroxyapatite has the ability to accommodate different ions to fulfil certain applications that affect bone

¹Department of Ceramics, National Research Centre, Cairo, Egypt

²Division of Biomaterials and Tissue Engineering, Eastman Dental Institute, UCL, London, UK

Corresponding author:

David YS Chau, Eastman Dental Institute, UCL, Division of Biomaterials and Tissue Engineering, Royal Free Hospital, Rowland Hill Street, London NW3 2PF, UK.

Email: d.chau@ucl.ac.uk



metabolism, bone growth or bone disease treatment.³ Both copper (Cu) and selenium (Se) ions are essential components for cell growth and proliferation. They also show a remarkable antibacterial activity impact.^{4–8} Unfortunately, the application of HA is severely constrained by its limited mechanical strength. A variety of polymeric substances, including gelatin (G) and chitosan (C), have been utilised as active polymer matrices.^{9,10} Polymeric components enable the regulated release of a medication and enhance mechanical qualities.

Gelatin (G) has good filmogenic qualities and water absorbing capacity, whereas chitosan (C) is regarded as a highly advantageous material because of its outstanding biocompatibility, non-toxicity, antibacterial capabilities and haemostasis.^{11–13} Gelatin and chitosan are therefore combined to increase the biological activity of the material as well as benefitting from incorporation of the tripeptide adhesion protein sequence, arginine-glycine-aspartic acid (RGD) that encourages cell adhesion and migration.¹⁴ Moreover, the novel biocomposite is able to produce the affiliated polyelectrolyte complexes and cofactors.¹⁵ This combination of gelatin–chitosan in scaffolds, found their application in regeneration of different tissues; such as bone,¹⁶ cartilage¹⁷ and skin.¹⁸

Crosslinking is essential to keep the implant stable. Therefore, tannic acid which is a naturally occurring polyphenol contains five catechol groups and five pyrogallol groups, has received FDA approval.¹⁹ It has acceptable biological properties; such as anti-inflammatory, antioxidant and antibacterial effects, and naturally exhibits the feature of tissue adhesion, all with avoiding the risk of medication resistance.^{19,20} It is the appropriate candidate to be used as a natural crosslinking agent to create materials that are not cytotoxic. The role of tannic acid in the crosslinking process between gelatin and chitosan, occurs through the various interactions of the numerous phenolic groups.

When an avian egg is developing, eggshell membrane (E) functions as an analogous ECM. It has a fibrous network made up primarily of glucosamine, desmosin and type I, V and X collagens.^{21,22} Type X collagen works to obstruct matrix mineralisation without being calcified,^{23–26} creating regions within a tissue to safeguard cells involved in the mineralisation.²⁷ It has been used to treat injuries, for its antibacterial and antimicrobial properties to fend off bacterial invasion.²⁸

As such, this investigation focuses on the novel development of a biologically-derived scaffold composite scaffold consisting of gelatin, chitosan and the eggshell membrane via the use of a naturally-derived crosslinking agent. Intriguingly, these materials are often considered as ‘waste’ products from the food/manufacturing industries and, as such, repurposing them to attain a high-value (medical) product would have significant implications in sustainability and green technology. Taken together alongside

the incorporation of HA, Cu and Se, this research may offer a promising new family of materials for biomedical research and/or clinical applications that is, bone repair and regeneration.

Methods

Preparation of scaffolds

Selenium and/or copper substituted hydroxyapatite–gelatin–chitosan–eggshell membrane nanocomposite scaffolds, were obtained through the precipitation process of apatite crystals within the polymer solution. The product was further subjected to a freeze-drying process. Accordingly, two solutions were separately prepared; the first was made of gelatin type B (Merck KGaA, Germany) in distilled water, while the second of chitosan (Acros, USA) in 1% (v/v) acetic acid. Pieces of eggshell membrane were distributed in distilled water using a homogeniser at 2×10^4 rpm. Precursor solutions of stoichiometric HA and three different substituted ones: selenium substituted hydroxyapatite (SeHA); copper substituted hydroxyapatite (CuHA); selenium and copper substituted hydroxyapatite (SeCuHA) were prepared in molar concentrations through an aqueous precipitation method.²⁹ The starting materials were calcium carbonate (CaCO_3 , $\geq 99\%$), di-ammonium hydrogen phosphate ($(\text{NH}_4)_2\text{HPO}_4$, $\geq 99\%$), sodium selenite (Na_2SeO_3 , 99%) and copper sulphate pentahydrate ($\text{CuSO}_4 \cdot 5\text{H}_2\text{O}$, $\geq 98\%$), all were purchased from Merck KGaA, Germany. The nanocomposite scaffold is formed by directly mixing the gelatin solution and eggshell membrane emulsion followed by the simultaneous addition of the hydroxyapatite precursors in a concentration ratio of G:C:E:HA equals 5:5:3:5. Ammonia was added to the solution to keep the pH at 8.0. The $(\text{Ca}+\text{Cu})/(\text{P}+\text{Se})$ molar ratio for the reaction was 1.67. The mixture was left at 40°C under continuous stirring for 24 h. Then the mixture was added to a chitosan solution and left for further stirring at 40°C for 2 h. An aqueous solution of tannic acid (0.5% (w/v) in distilled water and 20% (w/w) based on chitosan) was added to the mixtures and stirred continuously for 30 min at room temperature. The mixtures were allowed to cool at 4°C for 3 days to provide a pathway for the polymer crosslinking. The produced mixtures were washed using distilled water before being frozen at -20°C , then dried using a lyophiliser to produce porous scaffolds. Following the above stated procedure, gelatin–chitosan–eggshell membrane scaffold (GCE) as a control, was prepared.

Characterisation of the scaffolds

The prepared scaffolds were examined by X-ray diffractometer (XRD) (Bruker D8 diffractometer, Germany) at an accelerating voltage of 40 kV utilising Cu K α radiation ($\lambda = 1.54184 \text{ \AA}$) and 35 mA. Whereas, the main constituting

groups of the prepared samples, were analysed at room temperature by a Fourier-transform infrared (FTIR) spectroscopy (Spectrum One, Perkin Elmer, Llanstrisant, United Kingdom) over the spectral region between 4000 and 500 cm^{-1} . Morphology of scaffolds and the size of the pores were examined under a field emission scanning electron microscope (FESEM) using a Zeiss Sigma 300 VP FESEM (Zeiss, Cambridge, UK) set to 10kV. The dried specimens were sputter-coated with palladium and gold (Polaron E5000, Quorum Technology, Laughton, UK) before examination.

In vitro cell culture using MC3T3-E1

The prepared scaffolds were subjected to biocompatibility assessment using the mouse-derived osteoblastic cell line, MC3T3-E1, (The European Collection of Authenticated Cell Cultures (ECACC), UK) and cultured in MEM- α medium containing 10% (v/v) FBS and 1% (v/v) P/S. The scaffolds were cut into 0.5 cm (diameter) discs using a circular craft punch and then placed in Costar™ Ultra-Low Attachment 96-well tissue culture plates (TCP), (Merck, Poole, UK) after sterilisation for 30 min using UV irradiation.

The metabolic activity of the cells was evaluated using the CellTiter® 96 Aqueous One Solution Cell Proliferation assay (Promega, Southampton, UK) according to the manufacturer's protocol. In summary, following 3 and 7 days of incubation, 50 μL of the culture media was removed from each well before being transferred into a new 96-well plate and retained for the LDH assay. For the proliferation assay, 20 μL of CellTiter One reagent was added to each well and incubated at 37°C for 90 min whilst wrapped in aluminium foil. Following incubation, the supernatant solution was transferred to a new plate and read at 490 nm using a Tecan Infinite M200 microplate reader (Tecan, Switzerland).

Lactate dehydrogenase (LDH) release from the cells was quantified using the CytoTox 96® Non-radioactive Cytotoxicity Assay kit (Promega, Southampton, UK). In total, 50 μL of Reagent A was added to 50 μL of media suspension in each well (transferred to new plate as previously described), which was then incubated and covered in aluminium foil at $\sim 19^\circ\text{C}$ for 30 min. Thereafter, 25 μL of stop solution was added to each well. The absorbance was immediately read using a Tecan Infinite M200 microplate reader (Tecan, Männedorf, Switzerland). In both case, wells containing only media/media and samples were utilised for each time point as a reagent blank/background control.

To support the quantitative assays, the Live/Dead™ Viability/Cytotoxicity Staining Kit (Thermo-Fisher, Gloucester, UK) was used to demonstrate the biocompatibility of the scaffold samples. A total of 100 μL of cells, at a density of 1.5×10^4 cells/mL, were seeded onto the

scaffolds in 24-well plates. At the relevant time point, the media was discarded, and the samples were rinsed with PBS. The stain was prepared by adding 20 μL of EthD-1 (2 mM) stock solution to 10 mL PBS, combined with 5 mL Calcein AM (4 mM) stock solution. After 3 and 5-days incubation, 100 μL of the stain was added to each sample and incubated ($\sim 19^\circ\text{C}$) for 20 min. The viability of the cells was observed using fluorescence microscopy (LEICA Instruments, Milton Keynes, UK) on Image Capture Pro software.

Statistical evaluation

One-way ANOVA, Bonferroni's Multiple Post-Test, Holm Comparison Test ($p < 0.05$), statistical tests were used to analyse the data. The calculated values are shown as means and standard deviations.

Results and discussion

The XRD patterns of the GCE and different hydroxyapatite powders within nanocomposite scaffolds prepared through a precipitation method, are shown in Figure 1(a) and (b). The distinguishing diffraction peaks associated with G and E were present in all the samples at $2\theta = 20^\circ$ and 29° , respectively, in Figure 1(a). Whereas the characteristic peaks of C occurring at 15.9° and 22.7° in GCE were shifted to 18° and 22° , respectively in HA-GCE and to 22.5° in the other nanocomposites. The developed nanoapatite patterns indicate a poorly crystallised phase according to the JCPDS standard data of 09-0432 without recording the existence of any other secondary phase (Figure 1(b)). The hydroxyapatite peaks at 25.7° and $\sim 31^\circ\text{--}33^\circ$ and at 49.3° , that were shifted to 49.7° , appeared with a varied degree of intensity, low or high according to the type of substituted ion; whether the Se and/or Cu.

The main chemical groups found in the raw E and the nanocomposite scaffolds were determined by FTIR spectroscopy. The spectra obtained, are shown in (Figure 2). The absorbance bands of E were identified in all spectra, showed some particularities regarding their intensities after scaffold formation. The characteristic bands of hydroxyapatite were observed in addition to those of gelatin and chitosan after impregnation with apatite precursors (in agreement with the XRD results). The FTIR spectra showed a decrease in the absorbance bands of the N–H amide at 1632 and 1522 cm^{-1} specific of the E fibres, together with the appearance of the characteristic asymmetric stretching vibrations bands of phosphate around 1018 cm^{-1} . The vibration bands at 564 and 598 cm^{-1} corresponding to the P–O bond confirm the formation of hydroxyapatite.³⁰ The band around 1308 cm^{-1} assigned to O–H stretching band of the E fibres, appeared in all nanocomposite scaffolds and with high intensity in the substituted hydroxyapatite-nanocomposites. This is an indication

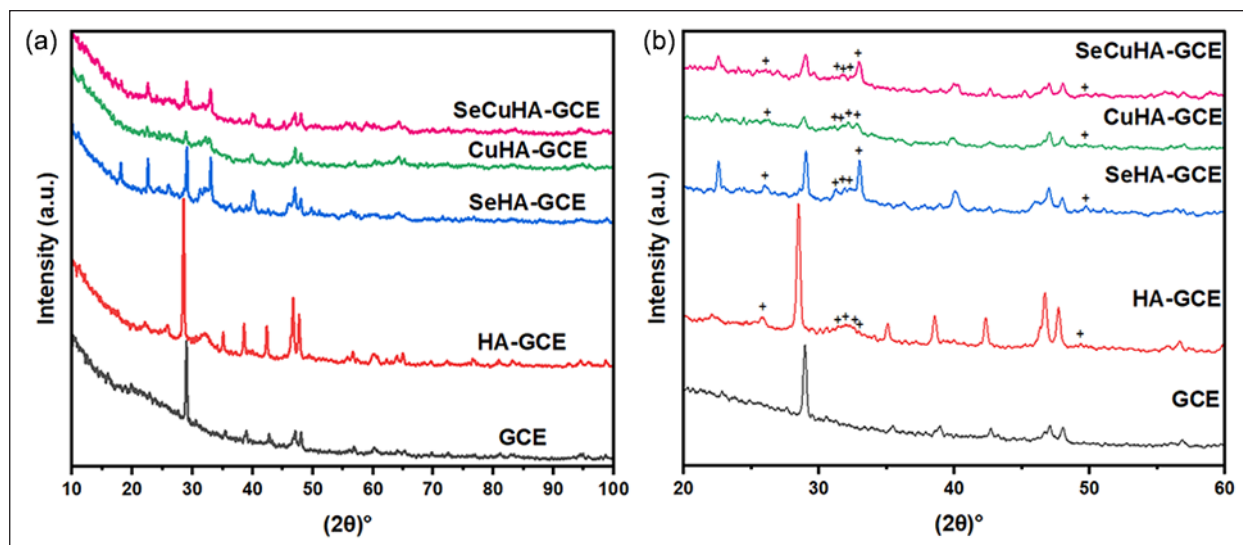


Figure 1. (a and b) XRD spectra of prepared control gelatin–chitosan–eggshell (GCE) membrane scaffold and nanocomposite scaffolds: hydroxyapatite-GCE (HA-GCE), selenium substituted hydroxyapatite-GCE (SeHA-GCE), copper substituted hydroxyapatite-GCE (CuHA-GCE) and selenium and copper substituted hydroxyapatite-GCE (SeCuHA-GCE). + corresponds to HA peaks.

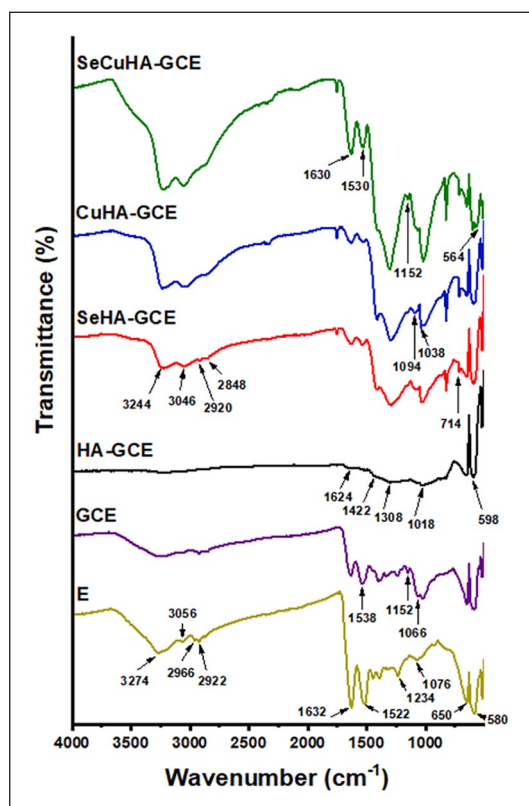


Figure 2. FTIR spectra of Eggshell membrane E and prepared control gelatin–chitosan–eggshell (GCE) membrane scaffold and nanocomposite scaffolds: hydroxyapatite-GCE (HA-GCE), selenium substituted hydroxyapatite-GCE (SeHA-GCE), copper substituted hydroxyapatite-GCE (CuHA-GCE) and selenium and copper substituted hydroxyapatite-GCE (SeCuHA-GCE).

of the existence of a hydrogen bond between E fibres and the formed apatite.^{31,32} The bands detected at 2922 and 2966 cm^{-1} are attributed to C–H stretching in E spectra.^{33,34} This band diminished or disappeared, in the nanocomposites spectra, suggesting the formation of hydroxyapatite nanoparticles on the E fibres. The bands at 3056 and 3274 cm^{-1} corresponding to the stretching mode of O–H and N–H groups of the E spectra appeared broader in the GCE spectra, while shifted to 3046 and 3244 cm^{-1} respectively in all the nanocomposites spectra. This might indicate a strong hydrogen bonding between the constituents. The band at 1076 cm^{-1} corresponding to S–O stretching vibration in E spectra is shifted to 1066 cm^{-1} in the GCE, and to around 1094 cm^{-1} with higher intensity in the CuHA-GCE, possibly due to the absorption appearance for the phosphate vibrational mode at 1038 cm^{-1} of the apatite component. The absorption band appeared at 1152 cm^{-1} in the GCE spectra is attributed to the chitosan saccharide structure³⁵ and was clearly detected in the spectra of SeCuHA-GCE. But it diminished in the HA-GCE and appeared as a shoulder band in the SeHA-GCE and CuHA-GCE, attributed to the interactions with the apatite components. The band at ~ 714 cm^{-1} may be a rocking vibration band due to the high degree of polymerisation and long molecular chain of polymers.³⁶

FESEM images of the GCE and nanocomposite scaffolds are displayed in Figure 3. The prepared scaffolds exhibit a porous structure made of E fibres embedded in a polymer network, and apatite particles evenly distributed over the pore walls gave the surface an aspect of being rough. The pore diameter of the GCE scaffold was in two

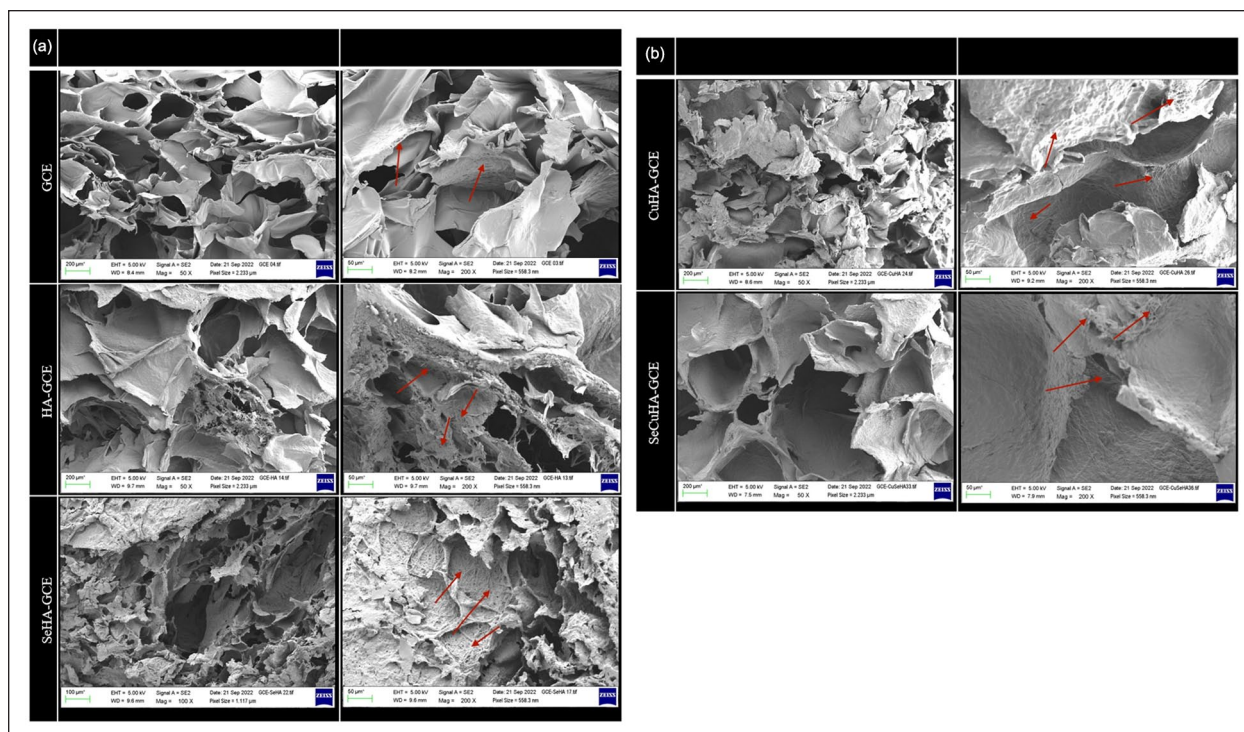


Figure 3. (a and b) FESEM images of prepared control gelatin–chitosan–eggshell (GCE) membrane scaffold and nanocomposite scaffolds: hydroxyapatite-GCE (HA-GCE), selenium substituted hydroxyapatite-GCE (SeHA-GCE), copper substituted hydroxyapatite-GCE (CuHA-GCE) and selenium and copper substituted hydroxyapatite-GCE (SeCuHA-GCE) at magnifications of 50, 100 and 200 X. Red arrows – dispersed E fibres.

ranges, the first between 118 and 407 μm and smaller ones between 28 and 84 μm . While the nanocomposite scaffold HA-GCE showed large pores with a diameter ranging between 122 and 420 μm besides small ones between 77 and 91 μm . SeHA-GCE scaffold showed the smallest pores with a diameter ranging between 110 and 190 μm and between 31 and 62 μm . Whereas the pores formed in CuHA-GCE scaffolds were between 145 and 200 μm and between 77 and 100 μm . The pores with the largest diameter were exhibited by SeCuHA-GCE scaffolds that were more uniformly distributed and had a diameter ranging from 166 to 680 μm , besides small ones ranging from 39 to 99 μm .

In it anticipated that the large pores in the scaffold will host cells as they will easily migrate towards/around and also fit inside, resulting in cell proliferation and/or differentiation – in the context of this work, towards the direct osteogenesis without first forming cartilage³⁷ – whereas the smaller pores are anticipated to allow nutrients to diffuse more easily throughout the scaffold.³⁸ The prepared nanocomposite scaffolds possessed sufficiently porous morphology with distributed apatite, that is vital for bone tissue engineering applications. Moreover, it is also possible that the scaffolds release the excipients either via scaffold degradation, weak binding of the elements, and/or weak cell interaction (e.g. phagocytosis, enzymatic interaction), therefore enhancing the biocompatibility/anti-tumour/anti-microbial characteristics of the scaffold.^{39–41}

MC3T3-E1 cell biocompatibility on the control GCE and nanocomposite scaffolds was evaluated using a simple metabolic activity assay (i.e. MTS), alongside a LDH expression profiling assessment for 3 and 7 days. On comparing the MTS and LDH assays results shown in Figure 4(a) and (b), respectively; it can be seen that the nanocomposite scaffolds demonstrated a higher metabolic activity and a lower expression of LDH than the GCE scaffold, suggesting that the cells found the former material to be eliciting a more (positive) biocompatible characteristic. This further suggests that the presence of the HA may be impacting cell viability and proliferation and most likely due to its association with increasing attachment and spreading of cells due to the enhancement/promotion of focal adhesion points, and cell signalling characteristics.⁴² Moreover, the nanocomposites containing hydroxyapatite with Se and/or Cu substitution demonstrated additional enhancement compared to the HA-GCE scaffold over same timepoints – suggesting that presence of Se and Cu further impact the growth and proliferation of cells. This observation is in agreement with a number of published studies and suggests that these elements play a significant role in the cell-cell and possibly cell-ECM interaction/signalling pathways.^{5–8} The fluorescence images from the Live-Dead staining assay for the MC3T3-E1 cells cultured on different scaffolds for 7 days (Figure 5) are in agreement with the observations

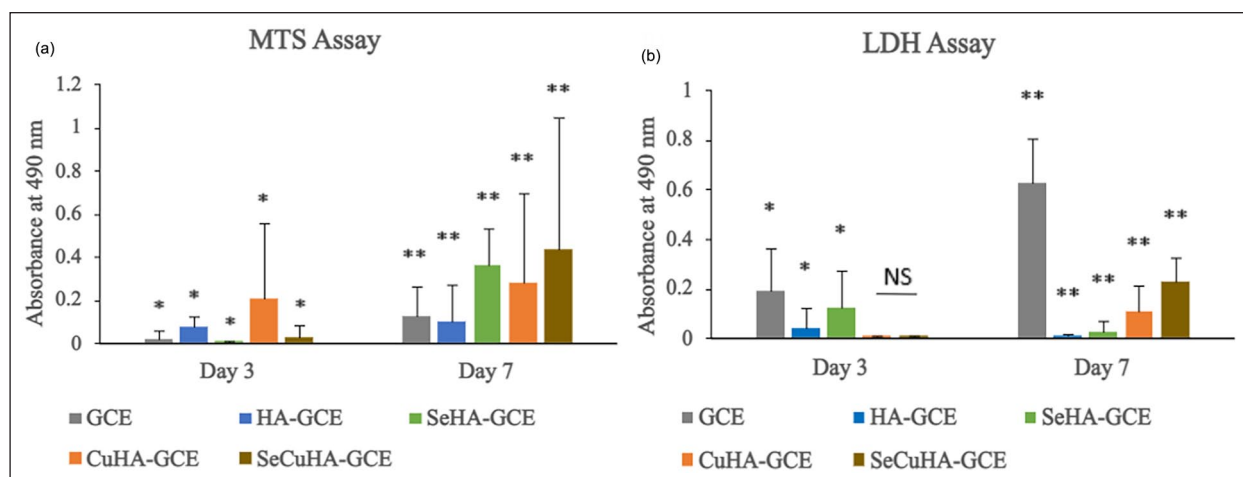


Figure 4. (a) Cell metabolic activity of MC3T3-E1 cells cultured on control gelatin–chitosan–eggshell (GCE) membrane scaffold and nanocomposite scaffolds: hydroxyapatite-GCE (HA-GCE), selenium substituted hydroxyapatite-GCE (SeHA-GCE), copper substituted hydroxyapatite-GCE (CuHA-GCE) and selenium and copper substituted hydroxyapatite-GCE (SeCuHA-GCE) after incubation for 3 and 7 days. (b) LDH release of MC3T3-E1 cells cultured on tissue culture plate (control) and different HA powders samples after incubated for 3 days. Data are represented as mean SD ($n=3$) with statistical assessment performed by using the one-way ANOVA with Bonferroni's Multiple Comparison Post Test and Holm Comparison Test. All pairs simultaneously compared, and they are significantly differenced with the p value <0.01 over each the day 3 (*) and day 7 (**). NS: no significant difference.

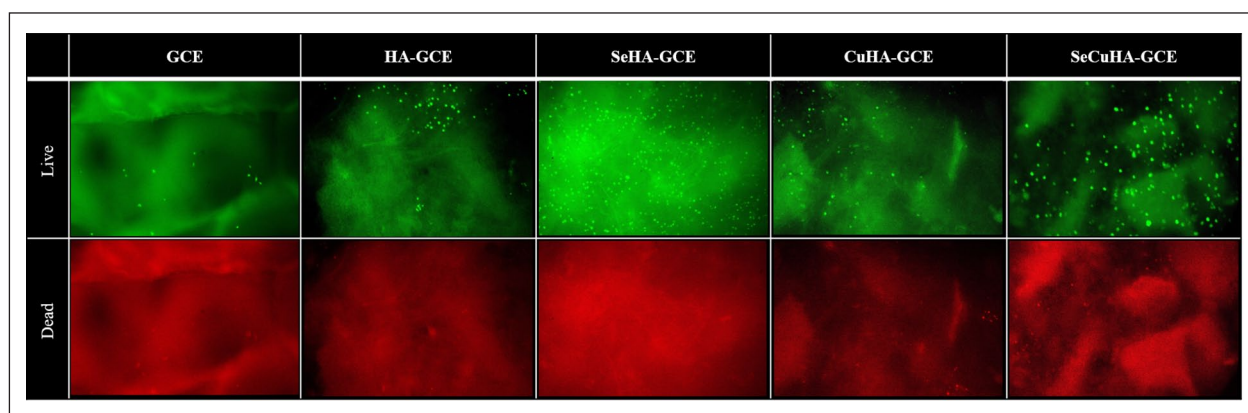


Figure 5. Fluorescence microscopy images of control gelatin–chitosan–eggshell (GCE) membrane scaffold and nanocomposite scaffolds: hydroxyapatite-GCE (HA-GCE), selenium substituted hydroxyapatite-GCE (SeHA-GCE), copper substituted hydroxyapatite-GCE (CuHA-GCE) and selenium and copper substituted hydroxyapatite-GCE (SeCuHA-GCE) with MC3T3-E1 cells cultured for 7 days (after live/dead assay). Living cells are stained green, dead cells are stained red. Upper row corresponding to “live” and lower row corresponding to “dead”.

seen in the MTS and LDH characterisation (Figure 4(a) and (b)), highlighting the fact that SeHA-GCE and SeCuHA-GCE scaffolds showed a greater population of viable cells and corresponding fewer dead cells than all other scaffolds. Moreover, the scaffold containing copper substituted hydroxyapatite, CuHA-GCE documented an even greater number of viable cells than the unsubstituted HA-containing scaffold. In control, the HA-GCE scaffold also documented a number of viable cells compared to those cultured on the unmodified GCE. In essence, the biological assessment of the materials indicate that the

studied scaffolds formed of Se- and/or Cu- substituted hydroxyapatite in situ embedded within the gelatin–chitosan–eggshell membrane promoted cell viability and proliferation of MC3T3-E1 cells.

Conclusions

Novel composite scaffold materials consisting of gelatin, chitosan and the eggshell membranes, crosslinked using tannic acid, and further infused with selenium and/or copper substituted hydroxyapatite nanoparticles were successfully

developed and optimised for reproducibility, as confirmed by XRD, SEM and FT-IR profiling. This novel technique which exploits a freeze-drying methodology without additional surfactants alongside the in situ precipitation of hydroxyapatite (with the different substitutions) also suggests the feasibility of developing further additional scaffolds with unique characteristics. Biocompatibility of the developed scaffolds was also validated using cell culture, and a minimal adverse effect was observed alongside a sustained viability profile with preosteoblasts. The addition of hydroxyapatite nanoparticles to the scaffold matrix produced a nano-topographically rough surface that improved cellular adhesion and proliferation. Taken together, these results suggest that the biocomposites, particularly when combined with the Se- and/or Cu-, offer a promising approach to the repair and regeneration of hard tissue that is, bone.

Acknowledgements

The authors appreciate the technical help provided by Dr Nicola Mordan, Dr George Georgiou, and Dr Graham Palmer.

Author contributions

Conceptualisation, SK, DI, DC; Methodology, SK, NS; Software, SK; Validation, SK, NS, DI, DC; Formal Analysis, SK, NS; Investigation, SK; Resources, DI, DC; Data Curation, SK; Writing – Original Draft Preparation, SK; Writing—Review and Editing, SK, NS, DI, DC.; Visualisation, SK; Supervision, DI, DC; Project Administration, DI, DC; Funding Acquisition, DC. All authors have read and agreed to the published version of the manuscript.

Declaration of conflicting interests

The author(s) declared no potential conflicts of interest with respect to the research, authorship, and/or publication of this article.

Funding

The author(s) disclosed receipt of the following financial support for the research, authorship, and/or publication of this article: This study was supported by grants from the RosetreesTrust [SeedcornAward], the Stoneygate Trust, as well as the Daniel Turnberg Travel Fellowship (DTTFR12\1129) Academy of Medical Sciences.

Guarantor

DC

ORCID iD

David YS Chau  <https://orcid.org/0000-0001-9200-6749>

References

- Wang P, Zhao L, Liu J, Weir MD, Zhou X and Xu HH. Bone tissue engineering via nanostructured calcium phosphate biomaterials and stem cells. *Bone Res* 2014; 2: 14017.
- Iafisco M and Catalucci D. Nano-apatites with designed chemistry and crystallinity for bone regeneration and nano-medical applications. In: Sprio S and Tampieri A (eds) *Bio-Inspired Regenerative Medicine*. Boca Raton, FL: CRC Press, 2016, pp.47–84.
- Šupová M. Substituted hydroxyapatites for biomedical applications: a review. *Ceram Int* 2015; 41: 9203–9231.
- Tran PL, Hammond AA, Mosley T, et al. Organoselenium coating on cellulose inhibits the formation of biofilms by *Pseudomonas aeruginosa* and *Staphylococcus aureus*. *Appl Environ Microbiol* 2009; 75: 3586–3592.
- Rodríguez-Valencia C, López-álvarez M, Cochón-Cores B, Pereiro I, Serra J and González P. Novel selenium-doped hydroxyapatite coatings for biomedical applications. *J Biomed Mater Res A* 2013; 101: 853–861.
- Korowash SI, Burdzinska A, Pędzisz P, et al. Selenium-substituted hydroxyapatite nanoparticles and their *in vitro* interaction on human bone marrow- and umbilical cord-derived mesenchymal stem cells. *Interceram – Int Ceram Rev* 2017; 66: 244–252.
- Gomes S, Vichery C, Descamps S, et al. Cu-doping of calcium phosphate bioceramics: from mechanism to the control of cytotoxicity. *Acta Biomater* 2018; 65: 462–474.
- Hu GF. Copper stimulates proliferation of human endothelial cells under culture. *J Cell Biochem* 1998; 69: 326–335.
- Shankar S, Wang LF and Rhim JW. Preparation and properties of carbohydrate-based composite films incorporated with CuO nanoparticles. *Carbohydr Polym* 2017; 169: 264–271.
- Shankar S, Teng X, Li G and Rhim JW. Preparation, characterization, and antimicrobial activity of gelatin/ZnO nanocomposite films. *Food Hydrocolloids* 2015; 45: 264–271.
- Archana D, Singh BK, Dutta J and Dutta PK. Chitosan-PVP-nano silver oxide wound dressing: *in vitro* and *in vivo* evaluation. *Int J Biol Macromol* 2015; 73: 49–57.
- Vimala K, Yallapu MM, Varaprasad K, et al. Fabrication of curcumin encapsulated chitosan-PVA silver nanocomposite films for improved antimicrobial activity. *J Biomater Nanobiotechnol* 2011; 02: 55–64.
- Kumar S, Dutta J and Dutta PK. Preparation and characterization of N-heterocyclic chitosan derivative based gels for biomedical applications. *Int J Biol Macromol* 2009; 45: 330–337.
- Ruoslahti E and Pierschbacher MD. New perspectives in cell adhesion: RGD and integrins. *Science* 1987; 238(4826): 491–497.
- Huang Y, Onyeri S, Siewe M, Moshfeghian A and Madhally SV. *In vitro* characterization of chitosan–gelatin scaffolds for tissue engineering. *Biomaterials* 2005; 26: 7616–7627.
- Yin Y, Ye F, Cui J, Zhang F, Li X and Yao K. Preparation and characterization of macroporous chitosan-gelatin/ β -tricalcium phosphate composite scaffolds for bone tissue engineering. *J Biomed Mater Res A* 2003; 67A: 844–855.
- Xia W, Liu W, Cui L, et al. Tissue engineering of cartilage with the use of chitosan-gelatin complex scaffolds. *J Biomed Mater Res* 2004; 71B: 373–380.
- Mao J, Zhao L, de Yao K, Shang Q, Yang G and Cao Y. Study of novel chitosan-gelatin artificial skin *in vitro*. *J Biomed Mater Res* 2003; 64A: 301–308.

19. Luo J, Yang J, Zheng X, et al. A highly stretchable, real-time self-healable hydrogel adhesive matrix for tissue patches and flexible electronics. *Adv Healthc Mater* 2020; 9: e1901423.
20. Yeo J, Lee J, Yoon S and Kim WJ. Tannic acid-based nanogel as an efficient anti-inflammatory agent. *Biomater Sci* 2020; 8: 1148–1159.
21. Osuji CI. Acid glycosaminoglycan of eggshell membranes. *Biochim Biophys Acta* 1971; 244: 481–483.
22. Wong M, Hendrix MJ, von der Mark K, Little C and Stern R. Collagen in the egg shell membranes of the hen. *Dev Biol* 1984; 104: 28–36.
23. Fujii S and Tamura T. Scanning electron microscopy of shell formation in hen's eggs. *J Fac Fish Anim Husb Hiroshima Univ* 1970; 9: 65–81.
24. Creger CR, Phillips H and Scott JT. Formation of an Egg Shell. *Poult Sci* 1976; 55: 1717–1723.
25. Stemberger BH, Mueller WJ and Leach RM. Microscopic study of the initial stages of egg shell calcification. *Poult Sci* 1977; 56: 537–543.
26. Baumgartner S, Brown DJ, Salevsky E and Leach RM. Copper deficiency in the laying hen. *J Nitr* 1978; 108: 804–811.
27. Arias JL, Nakamura O, Fernández MS, et al. Role of type X collagen on experimental mineralization of eggshell membranes. *Connect Tissue Res* 1997; 36: 21–33.
28. Ahlborn G and Sheldon BW. Enzymatic and microbiological inhibitory activity in eggshell membranes as influenced by layer strains and age and storage variables. *Poult Sci* 2005; 84: 1935–1941.
29. Jarcho M, Bolen CH, Thomas MB, Bobick J, Kay JF and Doremus RH. Hydroxylapatite synthesis and characterization in dense polycrystalline form. *J Mater Sci* 1976; 11: 2027–2035.
30. Fleet ME. The carbonate ion in hydroxyapatite: recent X-ray and infrared results. *Front Biosci* 2013; 5(2): 643–652.
31. Sundara Selvam PS, Chinnadurai GS, Ganesan D, Perumal P and Kandan V. Cadmium oxide-zinc oxide nanocomposites synthesized using waste eggshell membrane and its in-vitro assessments of the antimicrobial activities and minimum inhibitory concentration. *J Inorg Organomet Polym* 2021; 31: 816–835.
32. Feng C and Guo Y. Characterization of adsorptive capacity and mechanisms on adsorption of copper, lead and zinc by modified orange peel. *T Nonferr Met Soc* 2012; 22: 1224–1231.
33. Ertürk Avunduk AT and Bağlar S. Evaluation of microleakage in class v cavities prepared by different caries removal methods. *Microsc Res Tech* 2019; 82(9): 1566–1574.
34. Ballhuc S, Campian R, Labunet A, Negucioiu M, Buduru S and Kui A. Dental applications of systems based on hydroxyapatite Nanoparticles—An evidence-based update. *Crystals* 2021; 11(6): 674.
35. Naveen Kumar HMP, Prabhakar MN, Venkata Prasad C, et al. Compatibility studies of chitosan/PVA blend in 2% aqueous acetic acid solution at 30°C. *Carbohydr Polym* 2010; 82: 251–255.
36. Gómez-Lizárraga KK, Flores Morales C, Del Prado Audelo ML, Álvarez-Pérez MA, Piña-Barba MC and Escobedo C. Polycaprolactone and polycaprolactone/ceramic-based 3D-bioplotted porous scaffolds for bone regeneration: A comparative study. *Mater Sci Eng C Mater Biol Appl* 2017; 79: 326–335.
37. Karageorgiou V and Kaplan D. Porosity of 3D biomaterial scaffolds and osteogenesis. *Biomaterials* 2005; 26: 5474–5491.
38. Rajkumar M, Kavitha K, Prabhu M, Meenakshisundaram N and Rajendran V. Nanohydroxyapatite–chitosan–gelatin polyelectrolyte complex with enhanced mechanical and bioactivity. *Mater Sci Eng C* 2013; 33: 3237–3244.
39. Kargozar S, Mozafari M, Ghodrat S, Fiume E and Baino F. Copper-containing bioactive glasses and glass-ceramics: from tissue regeneration to cancer therapeutic strategies. *Mater Sci Eng C Mater Biol Appl* 2021; 121: 111741.
40. Zeng H, Cao JJ and Combs GF Jr. Selenium in bone health: roles in antioxidant protection and cell proliferation. *Nutrients* 2013; 5(1): 97–110.
41. Stolwijk JM, Garje R, Sieren JC, Buettner GR and Zakharia Y. Understanding the redox biology of selenium in the search of targeted cancer therapies. *Antioxidants* 2020; 9(5): 420.
42. Dan Y, Liu O, Liu Y, et al. Development of novel biocomposite scaffold of chitosan-gelatin/nanohydroxyapatite for potential bone tissue engineering applications. *Nanoscale Res Lett* 2016; 11: 487.